

# Turbulence and Rotation in Solar-Type Stars

V. A. Sheminova

Main Astronomical Observatory, National Academy of Sciences of Ukraine,  
Akademika Zabolotnoho 27, Kyiv, 03143 Ukraine  
e-mail: shem@mao.kiev.ua

## Abstract

Microturbulence, macroturbulence, thermal motion, and rotation contribute to the broadening of line profiles in stellar spectra. Reliable data on the velocity distribution of turbulent motions in stellar atmospheres are needed to interpret the spectra of solar-type stars unambiguously in exoplanetary research. Stellar spectra with a high resolution of 115000 obtained with the HARPS spectrograph provide an opportunity to examine turbulence velocities and their depth distributions in the photosphere of stars. Fourier analysis was performed for 17 iron lines in the spectra of 13 stars with an effective temperature of 4900–6200 K and a logarithm of surface gravity of 3.9–5.0 as well as in the spectrum of the Sun as a star. Models of stellar atmospheres were taken from the MARCS database. The standard concept of isotropic Gaussian microturbulence was assumed in this study. A satisfactory fit between the synthesized profiles of spectral lines and observational data verified the reliability of the Fourier method. The most likely estimates of turbulence velocities, the rotation velocity, and the iron abundance and their photospheric depth distribution profiles were obtained as a result. Microturbulence does not vary to any significant degree with depth, while macroturbulence has a marked depth dependence. The macroturbulence velocity increases with depth in the stellar atmosphere. The higher the effective temperature of a star and the stronger the surface gravity, the steeper the expected macroturbulence gradient. The mean macroturbulence velocity increases for stars with higher temperatures, weaker gravity, and faster rotation. The mean macro- and microturbulence velocities are correlated with each other and with the rotation velocity in the examined stars. The ratio between the macroturbulence velocity and the rotation velocity in solar-type stars varies from 1 (the hottest stars) to 1.7 (the coolest stars). The age dependence of the rotation velocity is more pronounced than that of the velocity of macroturbulent motions.

**Keywords:** line profiles, solar-type stars, velocity field, rotation, iron abundance, Fourier method

## 1 Introduction

Main-sequence F, G, and K solar-type stars are examined in this study. Nonthermal velocities (specifically, macroturbulence and rotation) are the primary cause of line profile broadening in the spectra of these stars. Macroturbulence is associated with granulation, supergranulation, oscillations, and other large-scale motions. The available measurement data [5, 6, 10, 14, 16, 17, 36, 43, 48] suggest that macroturbulent and rotation velocities for the indicated types of stars are comparable, produce the same effect on the shape of spectral-line profiles, and increase with effective temperature and luminosity. Reliable data on the changes in the macroturbulence with depth into stellar atmospheres are lacking, it is only known that the macroturbulence velocity values determined based on weak lines are higher than those determined for strong lines. The classical method of macroturbulence research is the comparative analysis of line profiles synthesized and observed in the wavelength scale. If the rotation parameters are not known beforehand, it is virtually impossible to determine macroturbulence velocities based on

line profiles. The Fourier method, which is more complex and is used less often than the classical method, provides an opportunity to estimate them.

The Fourier method was used in the 1970s by Gray and Smith [11, 12, 13, 14, 42, 43, 44]. The macrobroadening function was initially presented as a convolution of two functions: the rotation function, which depends on the position on the disk, and the isotropic macroturbulence function with the Gaussian model (GM). It was demonstrated in [12, 13] that the actual macroturbulence function has broader wings and a narrower core than the Gaussian function. The radial-tangential model (RTM) of velocities was proposed as an alternative, since macroturbulence is a manifestation of the granulation velocity field. Penetrative convection shapes a granulation pattern on the stellar surface by upward and downward convective flows and horizontal motions between them. Therefore, macroturbulence may be approximated by two flows directed along and transversally to the radius of a star. Experience showed that the RTM does not always provide a good fit to observational data. Later, Gray [16] presented a unified macrobroadening function incorporating rotation and macroturbulence effects. This function was calculated by integrating numerically over the stellar disk (see [18] for details). Once calculated, the macrobroadening function may be applied to different sets of observational data. In addition, averaging over several lines, one may derive a single solution defining the macroturbulence and rotation parameters. This approach is now used often [19, 20, 21].

Takeda [47] recently expressed doubts regarding the applicability of RTM to solar-type dwarf stars and presented the following arguments. The macroturbulence velocity for the Sun as a star determined in [13, 21] ( $\approx 4$  km/s) is significantly higher than the typical values of convective photospheric velocities (2–3 km/s) determined directly based on high-resolution spectroscopic data. It is also higher than the values for the center and the limb of the solar disk [23, 29, 38]. In order to clarify this issue, nonthermal velocities were studied in [47] by analyzing a large number of profiles of spectral lines, which were obtained in high-resolution observations in different parts of the solar disk using the procedure of profile fitting. It turned out that macroturbulence velocities follow an almost normal distribution without any signs of the special distribution expected in the RTM case. Takeda has concluded that the velocity field in the solar photosphere is more chaotic than in the RTM. It was also found that the classical anisotropic model  $\zeta_{\text{ma}}^2 = (\zeta_{\text{rad}} * \cos \theta)^2 + (\zeta_{\text{tan}} * \sin \theta)^2$ , where  $\zeta_{\text{rad}}$  and  $\zeta_{\text{tan}}$  are macroturbulence velocities with a Gaussian distribution in radial and tangential directions, serves as a good approximation of the macroturbulence velocity field in the solar photosphere. Using this model, Takeda has obtained  $\zeta_{\text{rad}} \approx 2$  km/s and  $\zeta_{\text{tan}} \approx 2.5$  km/s and concluded that the complex RTM is not suitable for characterizing macroturbulence in solar-type stars, while the classical GM is valid and convenient.

Fourier analysis with GM and RTM was performed in our previous study [40] to interpret the spectra of two stars and the solar flux. The obtained data did not reveal any clear advantages of RTM in the context of matching the velocity models to observational data. In our view, the simple Gaussian model is a reasonable (and even advantageous) alternative to RTM in routine spectral analysis of solar-type stars.

The aim of this study is to determine the micro- and macroturbulence velocities, the rotation velocity, and the iron abundance for 13 solar-type stars and to examine the depth profiles of turbulence velocities and the dependences of these velocities on the fundamental parameters of stars.

## 2 Analysis of the broadening of spectral lines

In order to analyze the broadening of line profiles in the spectra of slowly rotating solar-type stars, we have adapted the Fourier technique to the case when macroturbulence velocity  $\zeta$ , microturbulence velocity  $\xi$ , projection  $v \sin i$  of the rotation velocity, and element abundance  $A$  are the unknown parameters (see [40]). Let us outline the key stages of analysis.

It was assumed that thermal function  $H(\lambda)$  is independent of the position on the stellar disk, and observed line profile  $D(\lambda)$  may be represented by a double convolution:

$$D(\lambda) = H(\lambda) * M(\lambda) * I(\lambda). \quad (1)$$

Here,  $M(\lambda)$  is the macrobroadening function and  $I(\lambda)$  is the instrumental broadening function. Asterisks denote the convolution operation. Since convolution turns into multiplication in the Fourier domain, the Fourier transform of the observed profile is the product of the corresponding transforms

$$d(\sigma) = h(\sigma)m(\sigma)i(\sigma), \quad (2)$$

where  $\sigma$  [s/km] is the Fourier frequency and lower-case letters correspond to the transforms of functions from Eq. (1). Having divided the observed-line transform by thermal and instrumental transforms, we obtain the so-called residual transform:

$$m(\sigma) = d(\sigma)/h(\sigma)/i(\sigma), \quad (3)$$

which contains data on macrobroadening function  $M(\lambda)$ . In order to retrieve this data, one should define the model of velocities of macroturbulent motion and stellar rotation. Let us assume that the distribution of macroturbulence velocities is isotropic and may be represented by Gaussian function  $\Theta(\lambda)$  with the most likely macroturbulence velocity  $\zeta$ . Let us also assume that stellar rotation is of a solid-state nature and the rotation profile is set by the position-dependent classical rotation function  $G(\lambda)$  with parameter  $v \sin i$ . Function  $M(\lambda)$  is then a convolution of these two functions:

$$M(\lambda) = \Theta(\lambda) * G(\lambda). \quad (4)$$

Varying  $\zeta$  and  $v \sin i$ , one may find the best fit between the transform of function  $M(\lambda)$  and the residual transform in the noise-free frequency region and, thus, determine these two unknown parameters.

Thermal function  $H(\lambda)$  is easy to calculate using the standard procedure and the atmospheric models of stars obtained by interpolating data from the MARCS database [25]. Effective temperature  $T_{\text{eff}}$ , surface gravity  $\log g$ , and metallicity [M/H] were taken from [27]. The chemical composition of the Sun agreed with the data from [1]. The absorption coefficients were calculated in accordance with the SPANSAT algorithm [9], and the van der Waals damping constant was calculated using the Anstee-Barklem-O'Mara method [2, 3]. Since function  $H(\lambda)$  is a convolution of the Gaussian thermal profile with the Gaussian microturbulent profile, it depends on the most likely microturbulence velocity  $\xi$  and element abundance  $A$ . The values of these parameters are determined by comparing the calculated equivalent width of the thermal profile and the observed equivalent line width.

The following iterative procedure allows one to solve this problem with four unknown parameters: (0) transforms  $i(\sigma)$  and  $d(\sigma)$  are calculated; (1) initial value  $\xi = 0.5$  km/s is set, proper  $A$  is fitted, and  $H(\lambda)$ ,  $h(\sigma)$ , and  $m(\sigma)$  are calculated; (2) initial value  $V \sin i = 0.5$  km/s is set and a set of functions  $M(\lambda)$  and their transforms is calculated for  $\zeta = 0.5, 1.0, 1.5, 2.0, 2.5, 3.0$  km/s; (3) these transforms are compared with residual transform  $m(\sigma)$  and the minimum deviation is determined; (4) operations (2) and (3) are repeated for other values of  $V \sin i$  (1.0, 1.5, 2.0, 2.5, 3.0 km/s); (5) all operations starting from (1) are repeated for a different  $\xi$  value (1.0, 1.5, 2.0, 2.5 km/s); (6) the smallest minimum deviation, which defines all four unknown parameters, is found; (7) the line profile is calculated with the obtained values of  $\xi$ ,  $\zeta$ ,  $V \sin i$ , and  $A$  and is compared to the observed profile in the wavelength scale.

We have carefully selected a set of lines of neutral and ionized iron from the database [30] and the spectrum of the Sun as a star [26]. This list is rather small but remains unchanged for all stars (Table 1). The lines within it were checked for the availability of a blend-free profile

Table 1: Parameters of the spectral lines used, their equivalent widths and effective formation depths for the Sun.

$\lambda$ (nm)	$E_{\text{exp}}$ (eV)	$\log gf$	$W$ (nm)	$\log \tau_5$
FeI				
448.42198	3.603	-0.864	11.40	-1.70
460.20006	1.608	-3.154	7.71	-2.10
499.41295	0.915	-3.080	11.71	-2.62
524.24905	3.635	-0.968	9.43	-1.87
537.95734	3.695	-1.514	6.59	-1.59
550.14653	0.958	-3.047	12.22	-2.67
566.13455	4.285	-1.756	2.46	-1.00
570.54646	4.302	-1.355	4.15	-1.15
577.84533	2.588	-3.430	2.49	-1.23
606.54848	2.607	-1.530	12.88	-2.24
615.16170	2.175	-3.299	5.20	-1.63
625.25546	2.403	-1.687	13.50	-2.32
FeII				
450.82802	2.860	-2.440	9.53	-1.80
457.63330	2.840	-2.950	6.98	-1.53
523.46228	3.220	-2.180	9.18	-1.76
541.40730	3.223	-3.580	2.97	-0.90
645.63830	3.904	-2.050	6.72	-1.45

(at least one wing), accurate oscillator strengths, and parameters for calculating the damping constant. The lines were also chosen so as to maximize the range of depths of their formation. Their equivalent widths  $W$  for the studied stars fell within the range of  $260 > W > 20$  mÅ. Oscillator strengths  $\log gf$  with an error of 3–10% were taken from [7] for Fe I lines and from [32] for Fe II. The spectrum of the Sun as a star with a resolution of 300000 was taken from [26]. Stellar spectroscopic data derived from the results of observations [28] with the HARPS spectrograph mounted on the ESO 3.6 m Telescope at La Silla Observatory (Chile) were provided by Ya. Pavlenko and A. Ivanyuk. The signal-to-noise ratio and the resolving power of HARPS are higher than 100 and approximately equal to 115000, respectively.

The observed and model residual transforms were matched for each line individually so that the obtained velocity parameters could be tied to the depth of formation of a specific line, which was calculated using the depression contribution function in accordance with [24]. If macroturbulence is assumed to be independent of depth, the residual transforms for all lines of a given star should match, and an averaged residual transform may be used for fitting. In reality, the residual is affected by the imperfect line correction due to blends, errors in observation processing, and inaccuracies in choosing the continuum level and calculating the thermal profile. It was demonstrated in [19, 20, 21] that, despite the probable errors, the residual transform averaged over all lines yields a reliable result. Figure 1 demonstrates the observed symmetrized line profiles and their Fourier transforms for the Sun and HD 189627. The best fit between the residual line transforms is achieved at the lowest frequencies. The deviation increases at medium frequencies ( $-1.5 < \log \sigma < -1$ ) due to the macroturbulence velocity gradient. The spread for HD 189627 is even larger, since the corresponding spectral resolution and the signal-to-noise ratio of observations are lower. At higher frequencies ( $\log \sigma > -1$ ), observation noise is also intensified due to the fact that the observed transform is divided by the thermal one. We have compared the solution based on the averaged transform to the result averaged over all individual lines and obtained a satisfactory fit. Therefore, the use of an averaged residual transform should speed up the analysis considerably if one needs to obtain the parameters of turbulence velocities averaged over a large number of lines.

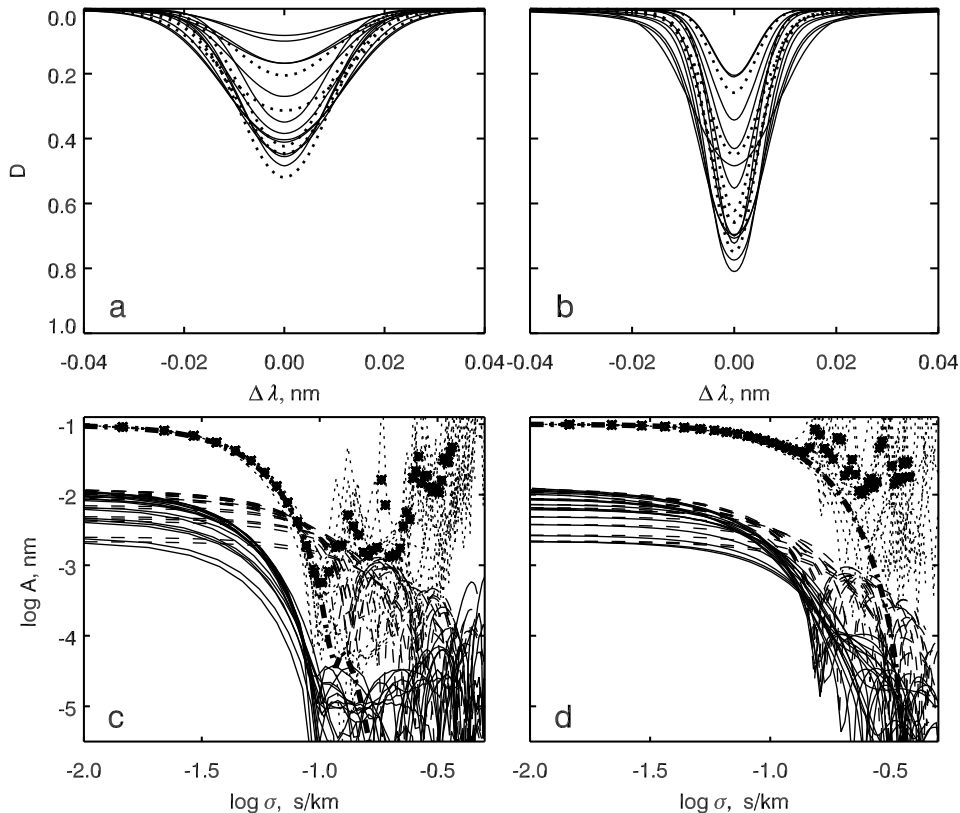


Fig. 1. Profiles  $D = 1 - F_\lambda/F_c$  of all the analyzed observed symmetrized Fe I (solid curves) and Fe II (dotted curves) lines for (a) the rapidly rotating star HD 189627 and (b) the Sun and amplitudes  $\log A$  of their Fourier transforms (solid curves), transforms of thermal profiles (dashed curves), residual transforms (dotted curves), averaged residual transform (asterisks), and modeled transform of the macrobroadening function (dash-and-dot curve) for (c) HD 189627 and (d) the Sun as functions of frequency  $\log \sigma$ .

### 3 Discussion

**Reliability of results.** The reliability in determination of turbulence velocities  $\zeta$  and  $\xi$ , projection  $V \sin i$  of the rotation velocity, and iron abundance  $A$  was verified for each line by directly comparing the calculated line profiles to observational data and finding the minimum deviation between them. It follows from Fig. 2 that the shapes of the mean deviation profile for almost all stars are similar. The observed profile is narrower at the center and has broader wings than the Gaussian profile. This actually validates the conclusion made by Gray regarding the deviation of line profiles from the Gaussian (bell) shape. Our data suggest that these deviations are small: they average to below 0.25% in the wings for all stars. The deviations for individual lines are as high as 1.5% for certain stars. This may be attributed to the presence of weak invisible blends or a slight asymmetry of the observed profiles (especially those corresponding to the Sun and cooler K stars). It also follows from Fig. 2 that the observed profiles are deeper at the line centers than the calculated profiles. This is true for the entire studied sample with the exception of three stars with the highest macroturbulence and rotation velocities, which exceed 5 km/s. The broader the lines are ( $V \sin i > 3$ ,  $\zeta > 3$  km/s), the more accurate reproduction of profile broadening is provided by the isotropic Gaussian macroturbulence distribution. We have also calculated line profiles with the GM macroturbulence distribution and the RTM distribution with integration over the disk and concluded that RTM provides only a slight improvement; the shape of the deviation profile remains hardly changed. Since the average deviations from observations remain within the accuracy of the present analysis, it is fair to assume that the obtained results are reliable.

Figure 3 presents the obtained values of macroturbulence velocity  $\zeta$ , microturbulence veloc-

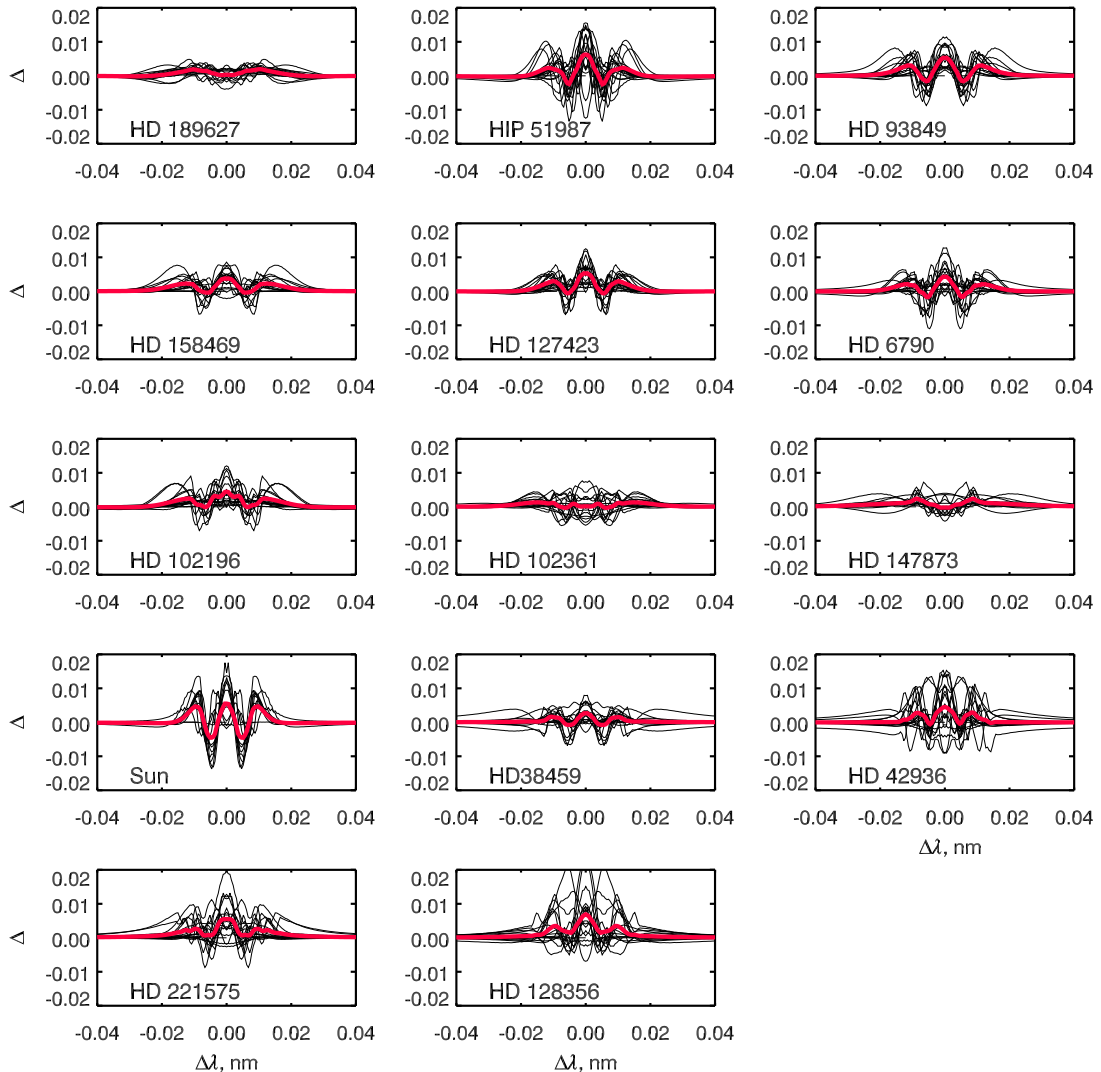


Fig. 2. Profiles of deviations  $\Delta$  between the observed  $D_{\text{obs}}$  and synthesized  $D_{\text{syn}}$  line profiles as functions of distance  $\Delta\lambda$  from the line center for all lines in each star. Bold red curves represent mean profiles of deviations. Line profiles were calculated as  $D = 1 - F_{\lambda}/F_c$ .

ity  $\xi$ , and iron abundance  $A = 12 + \log(N_{\text{Fe}}/N_{\text{H}})$  as functions of mean line formation depth  $\log \tau_5$ . The results for Fe I and Fe II lines do not feature any significant differences within the used MARCS atmospheric models. The results for each star were approximated with a linear dependence. Macroturbulence velocities have the maximum spread of values. A number of reasons for this may be suggested. The accuracy of Fourier analysis may be limited by the probable cross interference between  $V \sin i$  and  $\zeta$  in the comparison of residual transforms derived from the velocity model and observations. Weak anticorrelation between  $\zeta$  and  $\xi$  may be observed (it is noticeable for certain stars in Fig. 3). In addition, varying influences of macroturbulence and rotation may shape almost the same velocity profile. The large spread is also attributable to the fact that macroturbulence may depend both on the convective driving force and on other factors (e.g., magnetic field or other features of stellar activity that are neglected in the present analysis). Despite the mentioned drawbacks of the method, we managed to obtain reliable results by minimizing the deviation between model and observational data for a large number of lines.

The values of  $\zeta$ ,  $\xi$ ,  $V \sin i$ , and  $A$  averaged over all lines and their RMS deviations for each star are presented in Table 2 and Fig. 4. The RMS deviations are indicative of reliability of calculations (if there are no systematic variations of parameters with line intensity). These deviations were 0.10–0.32 km/s for  $\zeta$ , 0.05–0.12 km/s for  $\xi$ , 0.07–0.14 for  $A$ , and 0.02–0.05 km/s

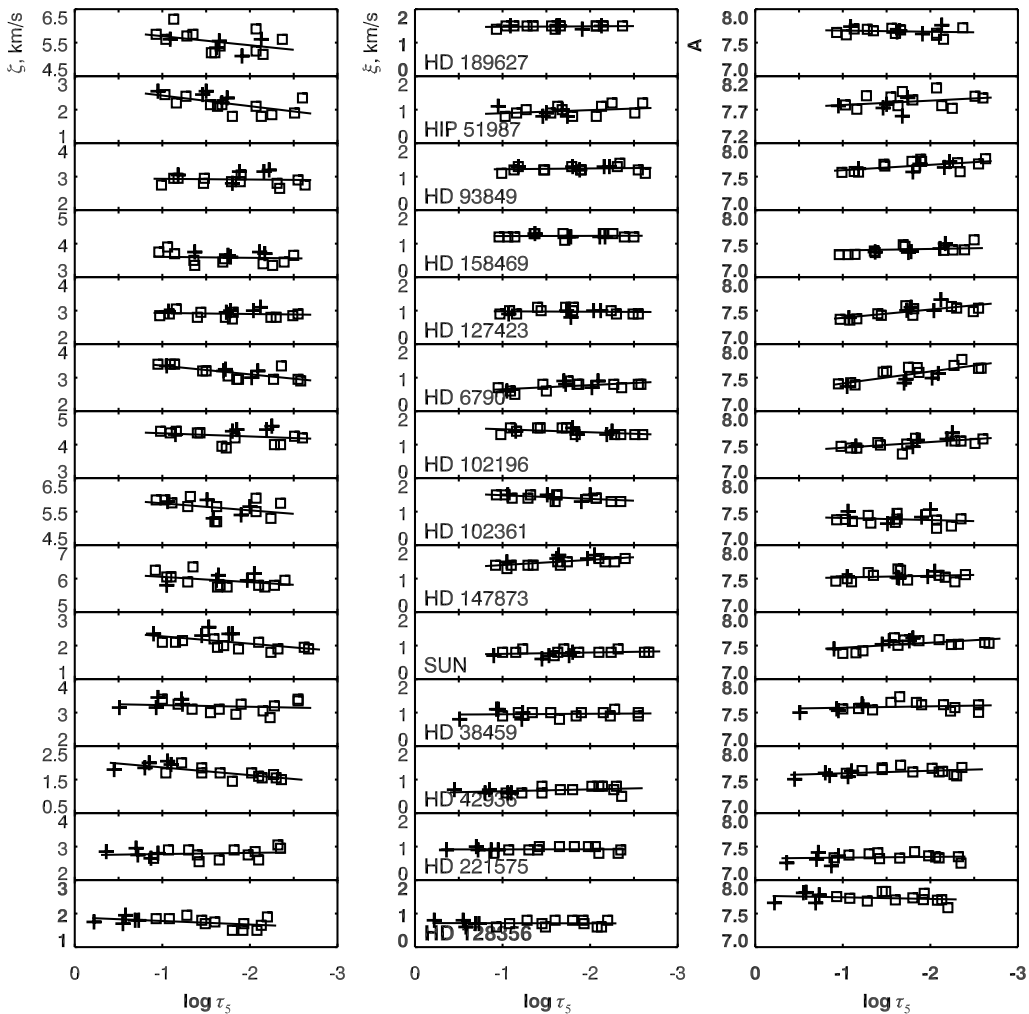


Fig. 3. Obtained values of macro-turbulence velocity  $\zeta$ , micro-turbulence velocity  $\xi$ , and iron abundance  $A = 12 + \log(N_{\text{Fe}}/N_{\text{H}})$  as functions of mean depth  $\log \tau_5$  of spectral-line formation. The data for Fe I and Fe II lines are denoted by squares and plus signs. Solid straight lines represent the results of linear approximation.

for  $V \sin i$ . The deviations for macro-turbulence were the largest, since  $\zeta$  depends on depth within the photosphere.

For the Sun as a star the obtained values of iron abundance  $A = 7.52 \pm 0.07$  dex, which agrees fairly well with the available data for the disk center ( $7.47 \pm 0.04$  dex [37]), and projection  $V \sin i = 1.84 \pm 0.02$  km/s, which matches the synodic rotation velocity of the Sun at the equator (1.84 km/s [21]), are indicative of reliability of the results of Fourier analysis.

**Variation of the obtained parameters with depth in the photosphere.** Our results suggest that macro-turbulence velocity  $\zeta$  varies with depth for most stars (Fig. 3). The most pronounced  $\zeta$  variations correspond to stars with higher effective temperatures and stronger gravity (i.e., in hotter, denser, and less extensive atmospheres). Being an indicator of convection in stars, macro-turbulence is related to the velocities of convective flows in subphotospheric and photospheric layers. The higher the convective velocities and the photosphere density, the steeper the gradient of  $\zeta$ . Therefore, stars with a more intense convection feature stronger macro-turbulence, and its variations with depth are more pronounced. The values of  $\zeta$  for the Sun as a star also clearly increases with depth. This has long been known from the studies of line profiles on the resolved solar disk [23, 29, 47].

It follows from Fig. 3 that micro-turbulence velocity  $\xi$  varies only slightly with depth. It is

Table 2: Parameters of the studied stars and the values of micro- and macroturbulence velocities, rotation velocity, and iron abundance determined via Fourier analysis and averaged over all lines.

Star	$T_{\text{eff}}$ (K)	$\log g$	[M/H]	$M/M_{\odot}$ [35]	Age $10^9$ , [35]	$\xi$ (km/s)	$\zeta$ (km/s)	$v \sin i$ (km/s)	$A$
HD 189627	6210	4.40	0.07	1.244	4.0	$1.48 \pm 0.04$	$5.52 \pm 0.30$	$5.93 \pm 0.02$	$7.67 \pm 0.05$
HIP 51987	6158	5.00	0.27	1.087	7.2	$0.96 \pm 0.14$	$2.20 \pm 0.25$	$2.09 \pm 0.03$	$7.81 \pm 0.10$
HD 93849	6153	4.21	0.08	1.268	3.5	$1.24 \pm 0.08$	$2.92 \pm 0.16$	$3.05 \pm 0.03$	$7.66 \pm 0.07$
HD 158469	6105	4.19	-0.14	1.223	2.0	$1.22 \pm 0.06$	$3.61 \pm 0.14$	$3.10 \pm 0.02$	$7.41 \pm 0.06$
HD 127423	6020	4.26	-0.09	1.107	3.1	$0.97 \pm 0.08$	$2.90 \pm 0.10$	$2.53 \pm 0.03$	$7.48 \pm 0.09$
HD 6790	6012	4.40	-0.06	1.089	3.5	$0.75 \pm 0.12$	$3.16 \pm 0.18$	$2.94 \pm 0.03$	$7.55 \pm 0.12$
HD 102196	6012	3.90	-0.05	1.395	3.0	$1.39 \pm 0.09$	$4.26 \pm 0.19$	$3.56 \pm 0.03$	$7.52 \pm 0.07$
HD 102361	5978	4.12	-0.15	1.250	2.0	$1.42 \pm 0.08$	$5.62 \pm 0.25$	$5.03 \pm 0.02$	$7.39 \pm 0.07$
HD 147873	5972	3.90	-0.09	1.493	2.6	$1.50 \pm 0.11$	$5.95 \pm 0.17$	$6.51 \pm 0.05$	$7.53 \pm 0.06$
Sun	5777	4.44	0.00	1.000	4.6	$0.78 \pm 0.08$	$2.11 \pm 0.21$	$1.84 \pm 0.02$	$7.52 \pm 0.07$
HD 38459	5233	4.43	0.06	0.882	9.0	$0.96 \pm 0.10$	$3.20 \pm 0.17$	$1.85 \pm 0.05$	$7.58 \pm 0.06$
HD 42936	5126	4.44	0.19	0.881	12.0	$0.68 \pm 0.09$	$1.74 \pm 0.18$	$0.97 \pm 0.03$	$7.61 \pm 0.05$
HD 221575	5037	4.49	-0.11	0.823	6.0	$0.92 \pm 0.07$	$2.79 \pm 0.14$	$1.89 \pm 0.03$	$7.34 \pm 0.06$
HD 128356	4875	4.58	0.34	0.824	15.5	$0.71 \pm 0.08$	$1.74 \pm 0.14$	$1.01 \pm 0.05$	$7.73 \pm 0.07$

fair to say that the gradients of microturbulence velocities for solar-type stars are insignificant. The value of  $\xi$  increases with depth for certain stars, decreases in another group of stars, and remains almost constant in the third group. The microturbulence velocity for the Sun as a star varies little with depth; according to our data, its mean value is  $0.8 \pm 0.1$ . According to the results of analysis for the center of the solar disk [22, 23, 29],  $\xi$  increases in deep photospheric layers and decreases with depth above the temperature minimum; its mean values for the center and the limb of the disk are  $\xi = 0.8\text{--}1.0$  and  $1.4\text{--}1.7$  km/s. It is likely that the effect of averaging over the disk masked the variation of  $\xi$  with depth. Gray [14] has pointed out that the data on variation of turbulence velocities with depth remain contradictory and do not allow one to draw definite conclusions.

Iron abundance  $A$  should not vary from one line to another and should not depend on depth in the photosphere. It follows from Fig. 3 that the values of  $A$  for certain stars and the Sun decrease with depth, while other stars do not manifest such a dependence. It may be noted that  $\xi$  and  $A$  are not anticorrelated and that the disregard for non-LTE effects is not the cause for variation of  $A$  with depth, since the values of  $A$  obtained for Fe I and Fe II lines agree with each other. The variation of iron abundance with depth is likely to be related to errors in determination of equivalent widths of the observed weak lines, which may be underestimated due to inaccurate setting of the continuum level. The equivalent widths of strong lines may be overestimated due to the presence of invisible and unaccounted blends in broader line wings.

The obtained values of rotation velocity  $V \sin i$  reveal hardly any variation from one line to the other in all stars; therefore, they are not shown in Fig. 3.

**Variation of the obtained parameters along the HR diagram.** The studied stars may be divided into two groups with effective temperatures of  $\approx 6000$  and  $\approx 5000$  K. Therefore, it is hard to identify a dependence on  $T_{\text{eff}}$  along the HR diagram. Figure 4 shows the values of  $\zeta$ ,  $\xi$ ,  $V \sin i$ , and  $A$  averaged over all lines for each star. The obtained turbulence velocities vary by a factor of two on average from the hottest stars to the coolest ones. In general,  $\zeta$ ,  $\xi$ , and  $V \sin i$  increase with temperature  $T_{\text{eff}}$  and mass  $M/M_{\odot}$  but become smaller as surface gravity  $\log g$ , metallicity [M/H], and the age of a star increase. It follows from Fig. 4 that the variation of  $V \sin i$  with age is the most pronounced; the age dependences of  $\zeta$  and  $\xi$  are weaker. These variation patterns agree with the ones determined earlier.

Figure 5 reveals an almost linear relationship between micro- and macroturbulence velocities:  $\zeta \approx 4.21\xi - 1.11$ . This is the reason why their dependencies on stellar parameters are similar. The macroturbulence velocity decreases from 4 km/s for hot stars to 2 km/s for cool stars; its solar value is 2.1 km/s. According to [15], the mean convective velocity decreases from 5.3 km/s



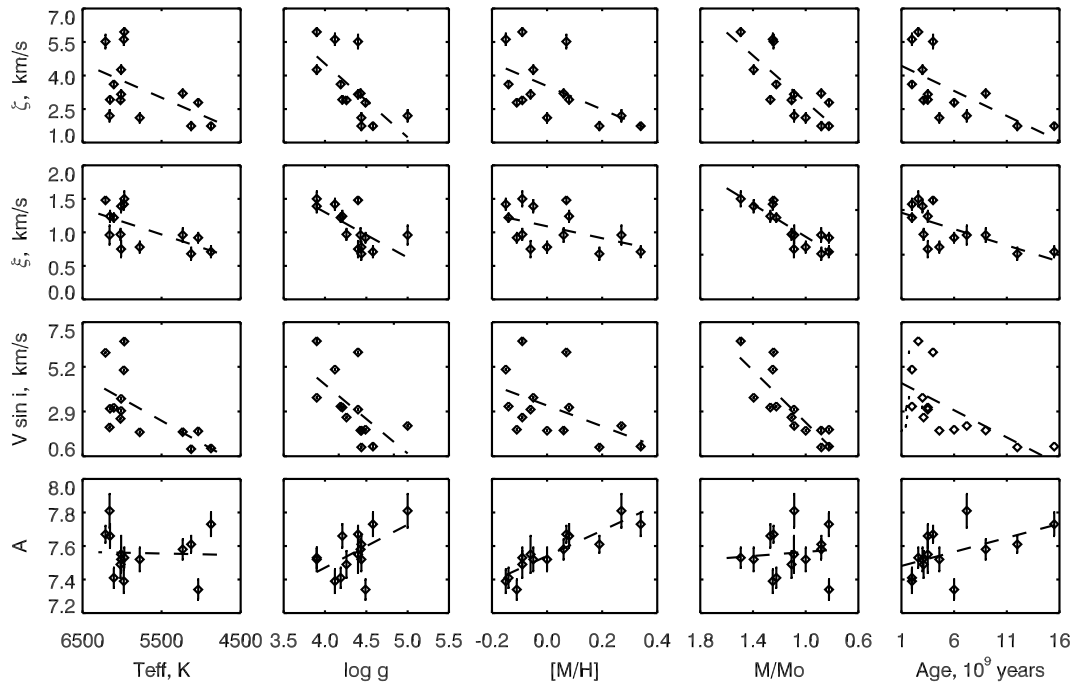


Fig. 4. Average values of macroturbulence velocity  $\zeta$ , microturbulence velocity  $\xi$ , rotation velocity  $V \sin i$ , and iron abundance  $A$  as functions of the key stellar parameters: effective temperature  $T_{\text{eff}}$ , surface gravity  $\log g$ , metallicity  $[M/H]$ , mass  $M/M_{\odot}$ , and age.

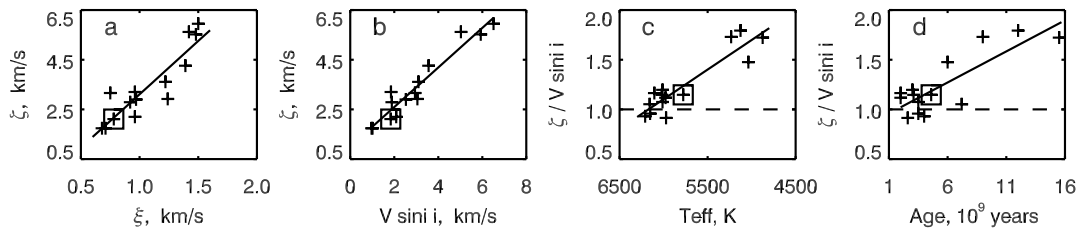


Fig. 5. Dependences of the average values of macroturbulence velocity  $\zeta$  on microturbulence velocity  $\xi$  and rotation velocity  $V \sin i$  and dependences of ratio  $\zeta/V \sin i$  on effective temperature  $T_{\text{eff}}$  and the age of a star. Squares represent data for the Sun.

in F5 V stars to a near-zero value in G8 V stars, but it increases again in even cooler stars. The convective velocity for the Sun is  $1.9 \pm 0.2$  km/s. The obtained values of  $\zeta$  for solar-type stars do not contradict the conclusions made in [15] regarding the proportionality between  $\zeta$  and convective velocities.

The spread of  $\zeta$  and  $\xi$  values in stars with equal effective temperatures is largely due to the differences in  $\log g$ . Turbulence velocities decrease as surface gravity  $\log g$  increases, since the photosphere becomes denser and thinner. The chemical composition of the photosphere (or metallicity) may also affect the temperature dependence. The higher the concentration of metals, the more opaque and denser the photosphere; as a result, turbulence gets weaker. A well-marked dependence of turbulence velocities on  $T_{\text{eff}}$  in FGK stars may be obtained only if the studied stars would have the same values of  $\log g$  and metallicity.

The results of our spectrometric measurements of  $V \sin i$  as a function of stellar parameters are presented in Fig. 4. It can be seen that the trends in variation of  $V \sin i$  and  $\zeta$  are similar. Apparently, this is a manifestation of the relation between macroturbulence and rotation through convection. Macroturbulence depends on the properties of convection, which is affected by stellar rotation. This rotation is the driving force behind magnetic activity in convective layers.

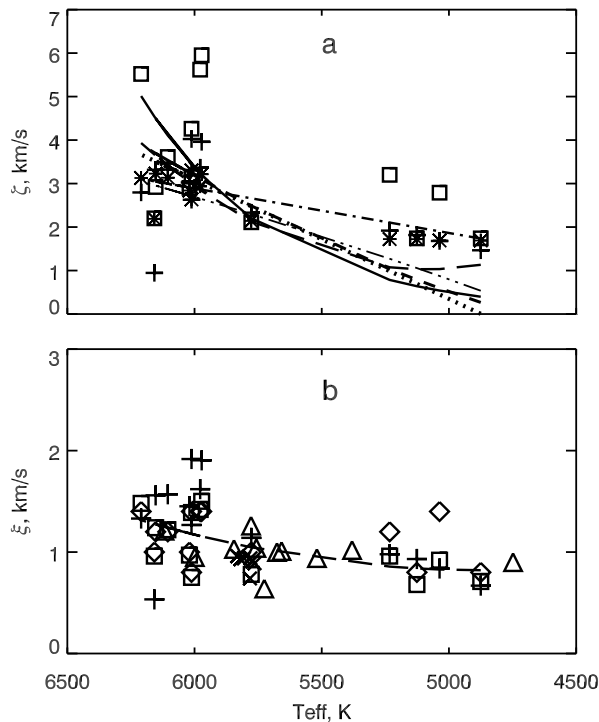


Fig. 6. Dependences of (a) macroturbulence velocity  $\zeta$  (squares correspond to data from this study; asterisks, Doyle et al. [6]; plus signs, Gonzalez [10]; dotted curve, Gray [17]; dash-and-dot curve, Saar & Osten [36]; dash-and-dot curve, Valenti & Fischer [48]; dashed curve, Bruntt et al. [5]; solid curve, Brewer et al. [4]; long dashed curve, Takeda & UeNo [47]) and (b) microturbulence velocity  $\xi$  (squares correspond to data from this study; plus signs, Nissen [34]; triangles, Neves et al. [33]; crosses, Sousa et al. [45]; diamonds, Ivanyuk et al. [27]; long dashed curve, Bruntt et al. [5]) on the effective temperature. All velocities  $\zeta$  are reduced to the scale of macroturbulence velocities with the Gaussian distribution ( $\zeta_G$ ).

Emerging magnetic fields give rise to the chromospheric activity. The reduction in rotation velocity at lower  $T_{\text{eff}}$  is usually attributed to the deceleration of rotation induced by mass ejections (stellar wind). The stellar wind of main-sequence F0 stars (and cooler ones) may be driven by convection and chromospheric activity. Thus, rotation has an effect on convection, and convection affects macroturbulence and, via the magnetic field and chromospheric activity, rotation. This validates the relationship between macroturbulence and rotation (Fig. 5), which may be represented by the following empirical formula:  $\zeta \approx 1.25 + 0.68 * V \sin i$ . It is also instructive to trace the variation of ratio  $\zeta/V \sin i$  with  $T_{\text{eff}}$  (Fig. 5). It can be seen that the average value of this ratio is 1 for hot stars and 1.7 for cooler K stars. Therefore, the macroturbulence velocity for solar-type stars decreases slower with age than the rotation velocity.

## 4 Comparison with the results of other studies

The macroturbulence velocity was determined in different studies with either the isotropic Gaussian model ( $\zeta_G$ ) or the radial-tangential model ( $\zeta_{\text{RT}}$ ). The ratio between  $\zeta_{\text{RT}}$  and  $\zeta_G$  values was estimated at  $\zeta_{\text{RT}}/\zeta_G = 1.44$  in [14] and  $\approx 1.5$  in [14] by fitting the Fourier transforms. Takeda [47] suggests that this ratio may depend on the additional line broadening. He obtained  $\approx 1.67$  by fitting line profiles for the solar flux. We have also determined  $\zeta_{\text{RT}}/\zeta_G$  by fitting the observed and calculated line profiles with RTM and GM and obtained a value of  $\approx 1.5$ , which was used to convert  $\zeta_{\text{RT}}$  into  $\zeta_G$  derived from line profiles. The value of  $\zeta_{\text{RT}}/\zeta_G = 1.44$  [14] was used to convert the  $\zeta_{\text{RT}}$  estimates derived from Fourier transforms.

Figure 6a shows the values of macroturbulence velocities in FGK stars determined in [4,

Table 3. Results of different studies focused on determining the parameters of turbulence velocities for the Sun as a star. Asterisks denote the values obtained by converting  $\zeta_{\text{RT}}$  to  $\zeta_{\text{G}}$  and vice versa.

$\zeta_{\text{RT}}, \text{km/s}$	$\zeta_{\text{G}}, \text{km/s}$	$\xi, \text{km/s}$	$V \sin i, \text{km/s}$	Method	Reference
			Very strong lines		
2.3	1.5*	0.5	2.0	Line profile	[46]
			Strong lines		
3.0*	2.0	0.5	1.9	Line profile	[47]
3.1	2.15*	0.5	1.9	Fourier transform	[13]
2.58*	1.72	1.07	1.9	Line profile	[8]
2.6	1.9	0.70	1.85	Fourier transform	[41]
2.89	1.99	0.85	1.75	Fourier transform	[40]
2.92*	2.03	0.78	1.84	Fourier transform	This study
			Weak lines		
3.45*	2.3	1.2	2.03	Line profile	[39]
3.7	2.5*	0.5	2.0	Line profile	[46]
3.45*	2.3	0.8	1.9	Line profile	[36]
3.45*	2.3	0.5	1.9	Line profile	[47]
3.8	2.64*	0.5	1.9	Fourier transform	[13]
3.77	2.6*	–	1.75	Fourier transform	[21]
3.22	2.22	0.85	1.75	Fourier transform	[40]
3.15*	2.19	0.78	1.84	Fourier transform	This study
			Strong and weak lines		
3.2	2.13*	–	2.2	Fourier transform	[43]
3.21	2.14*	0.85	1.9	Line profile	[6]
3.5	2.2*	0.40	1.7	Fourier transform	[10]

5, 6, 10, 17, 36, 47, 48] as functions of the effective temperature. It should be noted that the coincidence between all empirical curves after the conversion  $\zeta_{\text{RT}}$  to  $\zeta_{\text{G}}$  is considerably better than that in a similar plot of Takeda [47]. Figure 6b presents the estimates of microturbulence velocities obtained in [5, 27, 33, 34, 45]. Our estimates (squares) agree fairly well with the results of other studies, verify the reliability of our analysis, and lend credibility to the dependences revealed earlier.

The following facts regarding macroturbulence are already known [14, 18]. Macroturbulence velocity  $\zeta$  is a steeper function of the spectral type than microturbulence velocity  $\xi$ . Velocity  $\zeta$  decreases rapidly toward later spectral types from F0 to K0. The microturbulence velocity decreases with a large spread of values in the hotter region from A5 to G0 and then increases somewhat to K stars. The weaker the gravity on the stellar surface, the higher the turbulence velocities. The rotation velocity increases markedly along the main sequence from F stars (5–5 km/s) to B0–A0 stars ( $\approx 200$  km/s) and reaches the measurement limit for cool GK stars. Stars with lower luminosities have higher rotation velocities than main-sequence stars. All this is confirmed by the data on micro- and macroturbulence and rotation of solar-type stars obtained in the present study.

**Estimates for the Sun.** The Sun is a reference for studies of other stars, and the solar flux spectrum is often used to test the results. The recent data for the Sun as a star are presented in Table 3. The large spread of  $\zeta_{\text{RT}}$  and  $\zeta_{\text{G}}$  values is attributable primarily to the variation of macroturbulence with depth in the solar photosphere. The values of  $\zeta_{\text{G}}$  determined based on weak and strong lines are 2.2–2.6 and 1.9–2.0 km/s, respectively. The microturbulence velocity value falls within the range from 0.4 to 1.2 km/s and is independent of the line intensity. The most likely causes of discrepancies between the  $\xi$  estimates are the errors in determination of the observed equivalent widths, oscillator strengths, and the damping constant. Therefore, a large spread of turbulence velocity values is to be expected in the analysis of stellar spectra.

**Comparison between our data and the estimates from [27].** It is instructive to compare our data to the estimates obtained for the same stars. The spectra of 107 solar-type stars taken from a set of high-quality homogeneous observational data Jenkins et al. [28] were analyzed by A. Ivanyuk et al. [27], and the effective temperature, the surface gravity, and the chemical composition of these stars were determined. In addition, the microturbulence

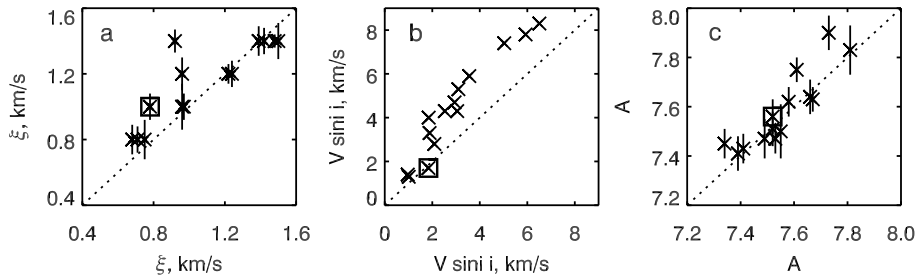


Fig. 7. Correlative dependences of the mean values of microturbulence  $\xi$ , rotation  $V \sin i$ , and iron abundance  $A$  obtained in [27] and in this study for the same stars. Squares represent the data for the Sun; the dotted line is the line of equal values.

velocity and the rotation parameter were estimated by analyzing the line profiles with a constant macroturbulence velocity  $\zeta_G = 2$  km/s assumed for all stars. This assumption may introduce a certain error into the obtained results, since macroturbulence depends on  $T_{\text{eff}}$  and  $\log g$ . Figure 7 shows the correlative dependences of  $\xi$ ,  $V \sin i$ , and iron abundance  $A$  estimated in the present study and in [27]. As expected, the values of  $V \sin i$  obtained in [27] are higher, since they compensate for the lack of macroturbulent broadening. The data on microturbulence velocity and iron abundance generally agree within the limits of error.

## 5 Conclusions

The line-of-sight turbulence velocities, the rotation velocity, and the iron abundance of solar-type stars were studied based on HARPS spectroscopic data. Fourier analysis with the isotropic Gaussian model of micro- and macroturbulence was performed for 17 iron lines in the spectra of 13 stars and the Sun. Since all properties of the atmosphere are defined by the energy flow and the gas density (or, in other words, by temperature and the surface gravity), the obtained results were tested for dependence on these parameters. The results of this test agreed in general with the dependences that were already known. We have also tried to determine the variation of turbulence velocities with depth in stellar atmospheres. The key findings are as follows.

The macroturbulence velocity in stellar atmospheres increases with effective temperature and with depth in the photosphere. It decreases as the surface gravity gets higher. The gradient of its variation with depth becomes steeper as the effective temperature increases and the surface gravity gets stronger. The macroturbulence velocity for the coolest stars is almost independent of depth.

The macroturbulence and microturbulence velocities are closely related. In general, microturbulence intensifies together with macroturbulence in the atmospheres of solar-type stars. The dependences of these velocities on the fundamental parameters are also similar; the only difference is that they are less steep for microturbulence. The microturbulence velocity varies little with depth in the atmospheres of the studied stars. It is almost constant for the Sun and several stars, while it either increases or decreases slightly with depth in other groups of stars.

The dependences of the projected rotation velocity on the effective temperature and the surface gravity are similar to those of the turbulence velocities. The higher the effective temperature and the lower the surface gravity, the faster the axial rotation of a star. The greater the age and the smaller the mass of a star, the lower the rotation velocity.

The stellar rotation velocity is correlated with macroturbulence. The higher the rotation velocity, the higher the macroturbulence velocity. The ratio between the macroturbulence and rotation velocities is approximately equal to unity for stars with an effective temperature of  $\approx 6000$  K. This ratio for cooler stars with an effective temperature of  $\approx 5000$  K is 1.7. The age dependence of the rotation velocity is more pronounced than that of the velocity of macroturbulent motions.

**Acknowledgments.** I thank Ya. Pavlenko and A. Ivanyuk for providing stellar spectra and for fruitful discussions.

**Funding.** This study was funded as part of the routine financing program for institutes of the National Academy of Sciences of Ukraine.

## References

- [1] Asplund, M., Grevesse, N., Sauval, A. J. The Solar Chemical Composition. *ASP Conf. Ser.* 2005. 336. P. 25–38.
- [2] Barklem P. S., Aspelund-Johansson, J. The broadening of Fe II lines by neutral hydrogen collisions. *Astron. Astrophys.* 2005. 435. P. 373–377.
- [3] Barklem P. S., Piskunov N., O’Mara B. J. A list of data for the broadening of metallic lines by neutral hydrogen collisions. *Astron. Astrophys. Suppl.* 2000. 142. P. 467–473.
- [4] Brewer J. M., Fischer D. A., Valenti J. A., Piskunov. N. Spectral Properties of Cool Stars: Extended Abundance Analysis of 1,617 Planet-search Stars. *Astrophys. J.* 2016. 225. Id. 32. 36 p.
- [5] Bruntt H., Bedding T. R., Quirion P.-O., Lo Curto G., Carrier F., Smalley B., Dall T. H., Arentoft T., Bazot M., Butler R. P. Accurate fundamental parameters for 23 bright solar-type stars. *Mon. Not. Roy. Astron. Soc.* 2010. 405. P. 1907–1923.
- [6] Doyle A. P., Davies G. R., Smalley B., Chaplin W. J., Elsworth Y. Determining stellar macroturbulence using asteroseismic rotational velocities from Kepler. *Mon. Not. Roy. Astron. Soc.* 2014. 444. P. 3592–3602.
- [7] Fuhr J. R., Wiese W. L. A Critical Compilation of Atomic Transition Probabilities for Neutral and Singly Ionized Iron. *Journal of Physical and Chemical Reference Data.* 2006. 35. P. 1669–1809.
- [8] Gadun A. S., Kostyk R. I. Analysis of Absorption Line Profiles in the Spectra of the Sun and Procyon – Velocity Field and Size of Inhomogeneities. *Soviet Astron.* 1990.34. N 3. P. 260–263.
- [9] Gadun A. S., Sheminova V. A. SPANSAT: the Program for LTE Calculations of Absorption Line Profiles in Stellar Atmospheres. – Kiev, 1988.-37 p.-(Preprint of the Institute for Theoretical Physics of Academy of Sciences of USSR, ITF-88-87P).
- [10] Gonzalez G. Spectroscopic analyses of the parent stars of extrasolar planetary system candidates. *Astron. Astrophys.* 1998. 334. P. 221–238.
- [11] Gray D. F. On the Existence of Classical Microturbulence. *Astrophys. J.* 1973. 184. P. 461–472.
- [12] Gray D. F. Atmospheric turbulence measured in stars above the main sequence. *Astrophys. J.* 1975. 02. P. 148–164.
- [13] Gray D. F. A test of the micro-macroturbulence model on the solar flux spectrum. *Astrophys. J.* 1977. 218. P. 530–538.
- [14] Gray D. F. Turbulence in stellar atmospheres. *Solar Phys.* 1978. 59. P. 193–236.

- [15] Gray D. F. Observations of spectral line asymmetries and convective velocities in F, G, and K stars. *Astrophys. J.* 1982. 255. P. 200–209.
- [16] Gray D. F. The temperature dependence of rotation and turbulence in giant stars. *Astrophys. J.* 1982. 262. N 2. P. 682–699.
- [17] Gray D. F. Measurements of rotation and turbulence in F, G, and K dwarfs stars. *Astrophys. J.* 1984. 281. P. 719–722.
- [18] Gray D. F. The Observation and Analysis of Stellar Photospheres. 3rd Edition, by D.F. Gray. ISBN 0521851866, UK: Cambridge University Press. 2005. 484 p.
- [19] Gray D. F. The Stable K0 Giant Star  $\beta$  Gem. *Astrophys. J.* 2014. 796. N 4. Id. 88. 11 p.
- [20] Gray D. F. A Spectral-line Analysis of the G8 III Standard  $\varepsilon$  VIR. *Astrophys. J.* 2017. 845. Id. 62. 10 p.
- [21] Gray D. F. A Solar-flux Line-broadening Analysis. *Astrophys. J.* 2018. 857. Id. 139. 8 p.
- [22] Gurtovenko E. A., Ratnikova V. A. Study of microturbulence from equivalent widths of moderate and moderately strong Fe I lines. *Astromet. Astrof.* 1976. 30.P. 14–25.
- [23] Gurtovenko E. A., Sheminova V. A. 'Crossing' method for studying the turbulence in solar and stellar atmospheres. I – Application to the sun. *Solar Phys.* 1986. 106. P. 237–247.
- [24] Gurtovenko E. A., Sheminova V. A. Formation depths of Fraunhofer lines. arXiv:1505.00975. 2015. 35 p.
- [25] Gustafsson B., Edvardsson B., Eriksson K., Jorgensen U. G., Nordlund A., Plez B. A grid of MARCS model atmospheres for late-type stars. I. Methods and general properties. *Astron. Astrophys.* 2008. 486. P. 951–970.
- [26] Hinkle K., Wallace L. The Spectrum of Arcturus from the Infrared through the Ultraviolet in Astronomical Society of the Pacific Conference. Series. 336. Cosmic Abundances as Records of Stellar Evolution and Nucleosynthesis, eds. T. G. Barnes, F. N. Bash. 2005. 321 p.
- [27] Ivanyuk O. M., Jenkins J. S., Pavlenko Ya. V., Jones H. R. A., Pinfield D. J. The metal-rich abundance pattern – spectroscopic properties and abundances for 107 main-sequence stars. *Mon. Not. Roy. Astron. Soc.* 2017. 468. P. 4151–4169.
- [28] Jenkins J. S., Jones H. R. A., Gozdziewski K. First results from the Calan-Hertfordshire Extrasolar Planet Search: exoplanets and the discovery of an eccentric brown dwarf in the desert. *Mon. Not. Roy. Astron. Soc.* 2009. 398. P. 911–917.
- [29] Kostik R. I. Damping constant and turbulence in the solar atmosphere. *Solar Phys.* 1982. 78. P. 39–57.
- [30] Kupka F., Piskunov N., Ryabchikova T. A., Stempels H. C., Weiss W. W. VALD-2: Progress of the Vienna Atomic Line Data Base. *Astron. Astrophys. Suppl.* 1999. 138.P. 119–133.
- [31] Kurucz R. L. Atlas: a Computer Program for Calculating Model Stellar Atmospheres. 1970. SAO Special Report N309, Cambridge, 292 p.
- [32] Melendez J., Barbuy B., Both accurate and precise gf-values for Fe II lines. *Astron. Astrophys.* 2009. 497. P. 611–617.
- [33] Neves V., Santos N. C., Sousa S. G., Correia A. C. M., Israelian G. Chemical abundances of 451 stars from the HARPS GTO planet search program. Thin disc, thick disc, and planets. *Astron. Astrophys.* 2009. 497. P. 563–581.

- [34] Nissen P. E. Metal abundance and microturbulence in F0-G2 stars and the calibration of the Stromgren m1 index. *Astron. Astrophys.* 1981. 97. P. 145–156.
- [35] Pavlenko Y. V., Kaminsky B. M., Jenkins J. S. Ivanyuk O. M., Jones H. R. A., Lyubchik Y. P. Masses, Oxygen and Carbon abundances in CHEPS dwarf stars. *Astron. Astrophys.* 2019. 621. Id.A112. 13 p.
- [36] Saar S. H., Osten R. A. Rotation, turbulence and evidence for magnetic fields in southern dwarfs. *Mon. Not. Roy. Astron. Soc.* 1997. 284. P. 803–810.
- [37] Scott P., Asplund M., Grevesse N., Bergemann M., Sauval A. The elemental composition of the Sun. II. The iron group elements Sc to Ni. *Astron. Astrophys.* 2015. 537. Id.A26, 33 p.
- [38] Sheminova V. A. Determination of microturbulent and macroturbulent velocity and an improved evaluation of the damping constant from Fraunhofer line profiles. *Astrometriia i Astrofizika.* 1984. 51. P. 42–45.
- [39] Sheminova V. A. Turbulence in the photosphere of the sun as a star. III. Micro-macroturbulence. *Solnechnye dannye. Byul. Glav. Astr. Obs.* 1984. 8. P. 70–78.
- [40] Sheminova V. A. Fourier analysis of spectra of solar-type stars. *Kinem. Phys. Cel. Bod.* 2017. 33. P. 217–230.
- [41] Sheminova V. A., Gadun A. S. Fourier analysis of Fe I lines in the spectra of the Sun,  $\alpha$  Centauri A, Procyon, Arcturus, and Canopus. *Kinem. Phys. Cel. Bod.* 1998. 14. N 3. P. 169–179.
- [42] Smith M. A. Applications of Fourier analysis to broadening of stellar line profiles. IV. A technique for separating macroturbulence from rotation in solar-type stars. *Astrophys. J.* 1976. 208. P. 487–499.
- [43] Smith M. A. An anticorrelation between macroturbulence and age in G stars near the main sequence. *Astrophys. J.* 1978. 224. P. 584–594.
- [44] Smith M. A. Rotational studies of lower main-sequence stars. *Pub. Astron. Soc. Pacific* 1979. 91. P. 737–745.
- [45] Sousa S. G., Santos N. C., Israelian G., Lovis C., Mayor M., Lo Curto G., Udry S. Spectroscopic stellar parameters for 582 FGK stars in the HARPS volume-limited sample. Revising the metallicity-planet correlation. *Astron. Astrophys.* 2011. 533. Id.A141. 9 p.
- [46] Takeda Y. Analyses of line profiles in the solar flux spectrum for determining rotation and micro/macro turbulence. *Pub. Astron. Soc. Japan* 1995. 47. P. 337–354.
- [47] Takeda Y., UeNo S. Does the radial-tangential macroturbulence model adequately describe the spectral line broadening of solar-type stars? *Pub. Astron. Soc. Japan* 2017. 69. Id.46. 25 p.
- [48] Valenti J. A., Fischer, D. A. Spectroscopic Properties of Cool Stars (SPOCS). I. 1040 F, G, and K Dwarfs from Keck, Lick, and AAT Planet Search Programs. *Astrophys. J. Suppl.* 2005. 159. P. 141–166.